ENGINEERING TRANSACTIONS • *Engng. Trans.* • **64**, 4, 589–596, 2016
Polish Academy of Sciences • Institute of Fundamental Technological Research (IPPT PAN)
National Engineering School of Metz (ENIM) • Poznan University of Technology

Cracks in Interfaces and Around Their Junctions in WC/Co Composite

Eligiusz POSTEK[1)], Tomasz SADOWSKI[2)]

[1)] *Institute of Fundamental Technological Research*
Polish Academy of Sciences
Pawińskiego 5B, 02-106 Warsaw, Poland
e-mail: ewpostek@gmail.com

[2)] *Lublin University of Technology*
Department of Solid Mechanics
Nadbystrzycka 40, 20-865 Lublin, Poland

WC/Co ceramic metal-matrix composites are characterized by very high mechanical properties that allow for application of the composites mostly in production of different types of cutting tools. By combining in a composite structure a phase of brittle hard wolfram carbide (WC) grains with a metallic interface of cobalt (Co) that exhibits plastic properties, a geometrically complex microstructure with significantly different mechanical properties of the combined phases is created, see Fig. 1a.

The presence of the elastic-plastic interface material, i.e. Co binder, in the composite structure is the reason for initiation of technological defects – mainly material porosity. During material loading pores start to coalesce and finally one can observe creation of microcracks system distributed along interfaces.

The aim of the paper is to show the previously formulated model [1, 2] of the polycrystalline composite to be extended towards cracks development around the junctions of the interfaces. The obtained numerical results indicate that in the junctions high stress concentrations were observed, which leads to crack initiation and its further unstable propagation, and finally the composite failure.

Results indicate that the first crack appears close to the junction and that the load carrying capacity of the sample is overestimated if a crack model in the interfaces is not assumed.

Key words: metal-ceramic composite, interface elements, crack propagation at composite junctions.

1. Introduction

Porosity in Metal-Ceramic Composites (MCC), e.g. WC/Co, strongly influences the material response to different types of loading [2–6]. The behaviour of

considered composite is very complicated, because it contains very hard ceramic elastic grains (WC) and very soft with small thickness continuous interfaces made of Co containing a certain amount of porosity. It was proved in [3, 6, 7] that metal interfaces are soft enough to evolve under loading condition, i.e. failure occurs by ductile growth of interface cavities, which finally coalesce. Ductile failure of Co can be considered as a primary mechanism manifesting fracture resistance in the WC/Co composite.

The aim of the paper is investigation of the most strained places of internal polycrystalline structure which is subjected to uniaxial tension. In particular, the junctions of interfaces play the important role as for stress concentration and further crack propagation.

2. Numerical model and results

2.1. Material properties

The cobalt binder of the analysed MCC polycrystal was modelled using interface elements, which were introduced into the interfaces between the grains and into the junctions as well. The model of the material in the grains is assumed elastic because of very high strength of the grains. The intergranular layers are elastic-plastic, i.e. the material model agrees with the experimental studies presented in [6, 7].

The SEM photograph of the WC/Co is given in Fig. 1a. The Finite Element Analysis (FEA) discretisation reflects the system of grains and takes into account the separate discretisation of the grains and the interfaces, which is shown in Fig. 1b. Additionally, we show the detail of a junction between the intergranular layers, Fig. 1c. The computational model consists of 18882 linear 8-node bricks in the grains, 15690 linear 8-node bricks in the intergranular layers and 47407 linear 8 node interface elements. The scheme of the cohesive element

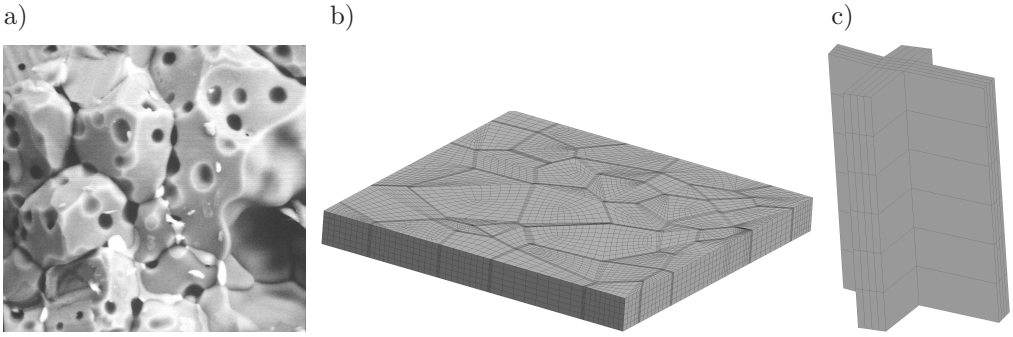

Fig. 1. SEM image of a WC-Co sample (a), FEA model of the sample (b), model of a junction (c).

is given in Fig. 2a. The discretisation generates 152 169 nodes. We use Abaqus program for FEA calculations [8]. We also use MSC Patran program [9] for the model building and GiD program for postprocessing and visualisation of the results [10].

a) b)

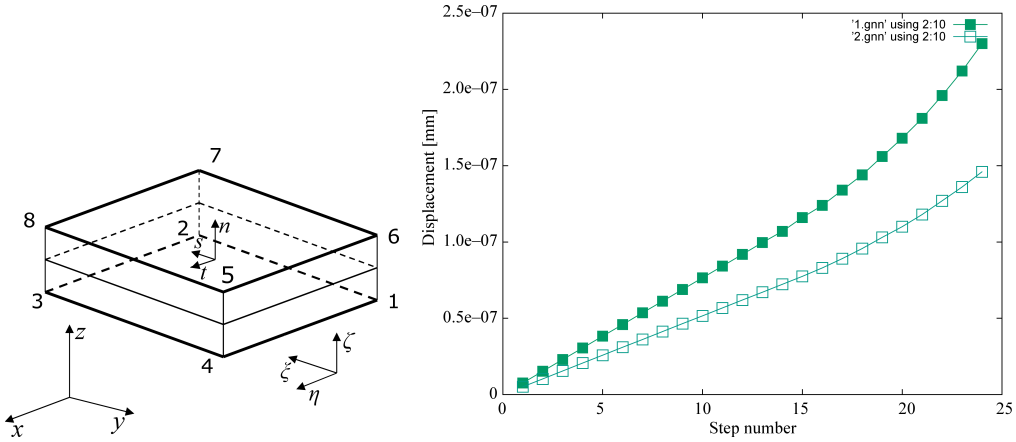

FIG. 2. 8-nodes cohesive element (a), horizontal displacement at the midspan of the left edge of the sample versus load step number for model with interface elements (filled squares) and without them (empty squares) (b).

The Young's modulus is $4.1 \cdot 10^{11}$ Pa and the Poisson's ratio is 0.25. The elastic material properties of the intergranular layers are: the Young's modulus $2.1 \cdot 10^{11}$ Pa and the Poison's ratio 0.235. The yield limit of the material is $2.97 \cdot 10^{8}$ Pa.

We assumed the possibility of the separation of the elements in the intergranular layers. We achieved the effect by introducing the cohesive elements around the elements in the interfaces. Following paper [11] we established the properties of the intergranular layers. We set the traction-separation model of the interfaces [12, 13].

The elastic properties of the interfaces are as follows: the elastic modulus normal to the interface (n) is $2.1 \cdot 10^{11}$ Pa, the shear moduli in the directions in plane of the interface $(s,\ t)$ are both $1.373 \cdot 10^{11}$ Pa. We assume the quadratic, strain formulated damage initiation condition that reads

$$\left\{\frac{\varepsilon_n}{\varepsilon_n^o}\right\}^2 + \left\{\frac{\varepsilon_s}{\varepsilon_s^o}\right\}^2 + \left\{\frac{\varepsilon_t}{\varepsilon_t^o}\right\}^2 = 1, \tag{2.1}$$

where ε_n is the nominal strain in the normal direction (n) to the interface, and ε_s, ε_t are the nominal strains in the two orthogonal (s) and (t) tangent directions to the interface. Moreover, ε_n^o, ε_s^o, ε_t^o are the maximum nominal strains at the

normal mode (n) and the shear modes in the directions (s) and (t). The modes are assumed to be separate. The values of the nominal strains are $2.5 \cdot 10^{-4}$, $6.65 \cdot 10^{-4}$ and 6.65×10^{-4}, respectively.

The maximum reduced stress due to isotropic damage reads [14]

$$\sigma^D_{\max} = \sigma_{\max}(1 - D). \tag{2.2}$$

The reduced stress depends on the non-dimensional damage variable $D = A/A_o$ where A is the damaged area and A_o is the initial area. The variable D varies between 0 and 1. It reflects the deterioration of the cross-section because of microcracks and microvoids that appear in the material during the loading process. The $\sigma_{\max}$ is the stress related to the current cross-section which means the undamaged area of the cross-section. The stress $\sigma^D_{\max}$ is the stress related to the pristine cross-section therefore it is the nominal stress.

We assumed an exponential softening rule. The damage variable evolution for this rule reads

$$D = 1 - \left(\frac{\delta^o_m}{\delta^{\max}_m}\right)\left(1 - \frac{1 - \exp\left(-\alpha\left(\frac{\delta^{\max}_m - \delta^o_m}{\delta^f_m - \delta^o_m}\right)\right)}{1 - \exp(-\alpha)}\right). \tag{2.3}$$

In the equation above, δ^o_m is the displacement when the applied stress reaches the maximum strength $(\sigma_{\max})$ at the initiation of damage, $\delta^{\max}_m$ is the maximum displacement in the loading history, δ^f_m is the displacement at failure, and α is the non-dimensional parameter of the rate of damage evolution.

2.2. Results

The sample is loaded with the normal pressure to the left side that extends the sample, Fig. 3. The structure is constrained in the x direction at the right side, and supported in the z direction on its entire bottom face. We follow the equilibrium path up to 480 MPa. The loading increases monotonously in 24 equal steps.

We note that the horizontal displacement of the node at the middle of the loaded edge of the sample grows faster for the sample with the introduced interfaces, Fig. 2b. This is due to early damage at the interfaces (step 2). The details we can observe in Fig. 4a and 4b. Additionally, we present the mesh of the interface elements in Fig. 4a.

We observe the qualitative difference in the displacement fields at the very beginning of the loading process, Fig. 3a, and at the end of the process Fig. 3b. The difference is significant. In the Fig. 3a, we can notice that the displacement field is quite regular and is only slightly disturbed at the intergranular layers

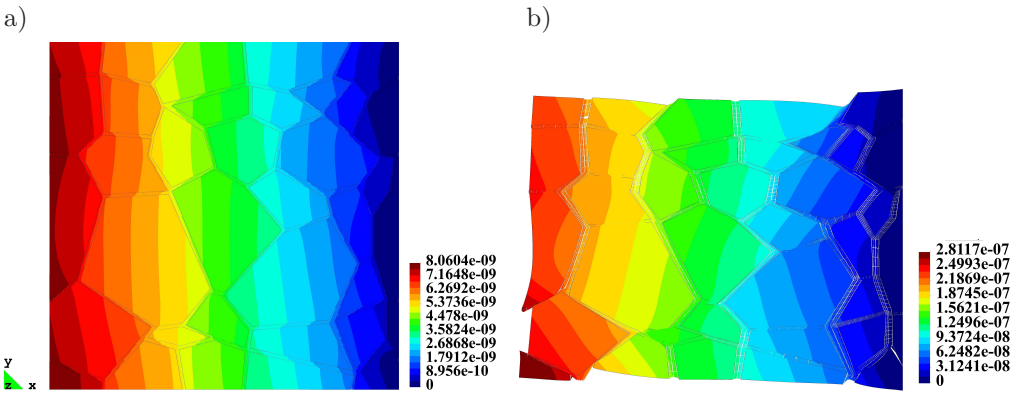

FIG. 3. Displacement fields after step 1 (a) and after 24 (b), scaled – ×100.

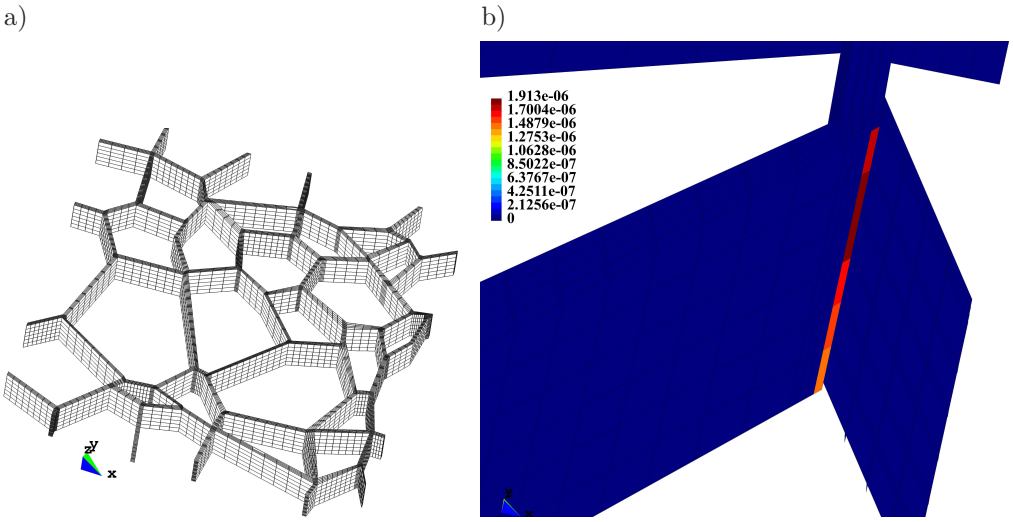

FIG. 4. Intergranular layers system with the cohesive elements discretisation (a) and the detail of the first damaged region (b).

bounds, while at the end of the process, the displacement field becomes irregular with distinct limits on the intergranular layers. It means that the grains are in relative movements. The grains slip along the layers. We can observe the cracks in the interfaces and between the interfaces and the grains. It is seen in the right lower part of the Fig. 3b particularly well. This is the region where the first cracks close to the junction appeared. It is demonstrated in Fig. 4b.

The observation of Fig. 5a and 5b shows that while the first yield appears (step 9) the damage zones are much more developed. It is valid for other regions of the sample, as well. We note qualitative difference of the Huber-Mises stress

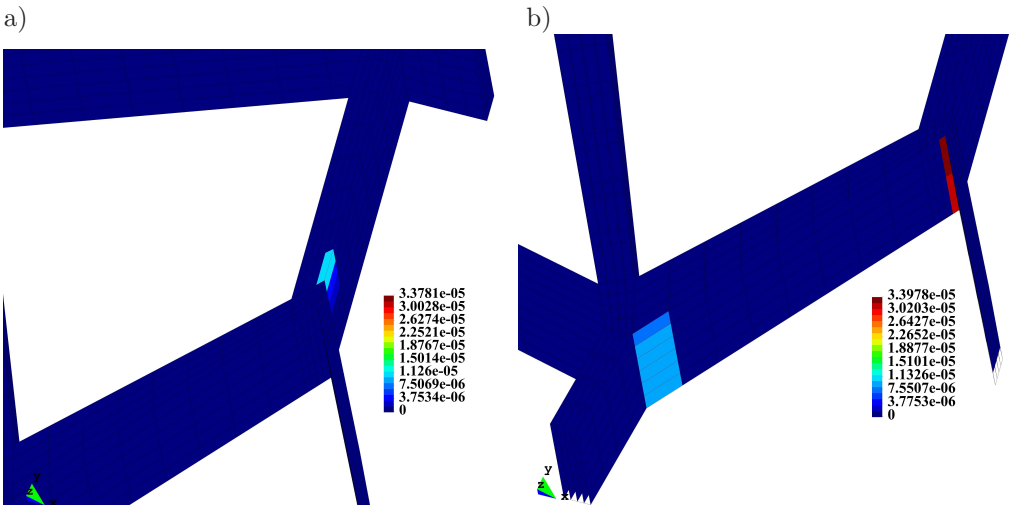

FIG. 5. First yield (a), damage distribution at the load level when the first yield appears (b).

distribution between the load level at the first yield, Fig. 6a, and close to failure, Fig. 6b. In the second case, the Huber-Mises stress distribution is quite uniform since in most of the intergranular layers plastic strains have appeared.

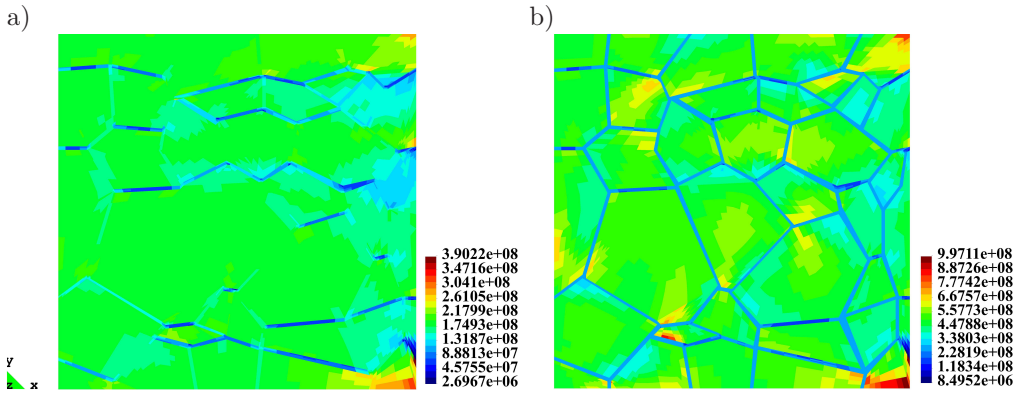

FIG. 6. Huber-Mises stress distribution at the load level when the first yield appears (a), Huber-Mises stress distribution at the end of the loading process (b).

3. Conclusion

We observed that the decohesion and slip in the interfaces appear earlier than the plastic strains. Therefore, we believe that a crack model should always be introduced when the load carrying capacity of the WC-Co samples is

investigated. If the crack model is not introduced the maximum loading is overestimated. We note that the first crack appears in the neighbourhood of the junction. We have also found that the computational model is rather effective due to its relative simplicity.

Acknowledgment

This work was financially supported by Ministry of Science and Higher Education (Poland) within the statutory research number S/20/2016 (Lublin University of Technology). The calculations were done at the Interdisciplinary Centre for Mathematical and Computational Modelling, University of Warsaw. The licence for the MSC Patran program was provided by Academic Computer Centre in Gdańsk.

References

1. Sadowski T., Hardy S., Postek E., *Prediction of the mechanical response of polycrystalline ceramics containing metallic intergranular layers under uniaxial tension*, Computational Materials Science, **34**(1): 46–63, 2005, doi: 10.1016/j.commatsci.2004.10.005.
2. Postek E., Sadowski T., *Assessing the influence of porosity in the deformation of metal-ceramic composites*, Composite Interfaces, **18**(1): 55–76, 2011, doi: 10.1163/092764410X554049.
3. Siegl L.S., Exner H.E., *Experimental study of the mechanics of fracture in WC-Co alloys*, Metallurgical Transactions A, **18**(7): 1299–1308, 1987, doi: 10.1007/BF02647199.
4. Dalgleish B.J., Lu M.C., Evans A.G., *The strength of ceramics bonded with metals*, Acta Metallurgica, **36**(8): 2029–2035, 1988, doi:10.1016/0001-6160(88)90304-5.
5. Sadowski T., Samborski S., *Development of damage state in porous ceramic under compression state*, Computational Materials Science, **43**(1): 75–81, 2008, doi: 10.1016/j.commatsci.2007.07.041.
6. Ravichandran K.S., *Fracture toughness of two phase WC-Co cermets*, Acta Metallurgica et Materialia, **42**(1): 143–150, 1994, doi: 10.1016/0956-7151(94)90057-4.
7. Dalgleish B.J., Trumble K.P., Evans A.G., *The strength and fracture of alumina bonded with aluminium alloys*, Acta Metallurgica, **37**(7): 1923–1931, 1989, doi: 10.1016/0001-6160(89)90077-1.
8. Abaqus 6.13. User's Manual.
9. http://www.mscsoftware.com/product/patran
10. http://www.gidhome.com/
11. Felten F., Schneider G.A., Sadowski T., *Estimation of R-curve in WC/Co cermet by CT test*, International Journal of Refractory Materials and Hard Materials, **26**(1): 55–60, 2008, 10.1016/j.ijrmhm.2007.01.005.

12. Camanho P.P., Dávila C.G., *Mixed-mode decohesion finite elements for the simulation of delamination in composite materials*, NASA Scientific and Technical Infomlation (STI) Program, NASA/TM-2002-211737, 2002, ntrs.nasa.gov/archive/nasa/casi.ntrs.nasa.gov/20020053651.pdf.

13. Zavattieri P.D., Hector L.G., Bower A.F., *Cohesive zone simulations of crack growth along a rough interface between two elastic-plastic solids*, Engineering Fracture Mechanics, **75**(15): 4309–4332, 2008, doi: 10.1016/j.engfracmech.2007.11.007.

14. Kachanov L.M., *Introduction to Continuum Damage Mechanics,* Martinun Nijhoff Publishers, Dordrecht, 1986.

Received October 15, 2016; accepted version November 16, 2016.